

Investigation of Various Organic Radicals Dispersed in Polymethylmethacrylate Matrices Using the Electron Spin Resonance Spectroscopy Technique

Hirokazu Kobayashi,* Kento Akiniwa, Fumiyasu Iwahori, Hidehiko Honda, Masato Yamamoto, Yuki Odanaka, and Masahiro Inagaki



Cite This: *ACS Omega* 2021, 6, 20855–20864



Read Online

ACCESS |



Metrics & More



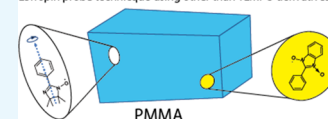
Article Recommendations



Supporting Information

ABSTRACT: The electron spin resonance (ESR) spectroscopy technique was used to study various organic radicals, such as 2,2,6,6-tetramethyl-1-piperidinyloxy (TEMPO), 4-hydroxy-TEMPO (TEMPOL), 2-*X*-nitronylnitroxide (2-*X*-NN, *X* = Ph, NO₂Ph, or cyclohexyl), 4-*Y*-benzoylnitronylnitroxide (4-*Y*-PhBzNN, *Y* = Ph or NO₂Ph), and 2-*Z*-iminonitroxide (2-*Z*-IN, *Z* = Ph or NO₂Ph) dispersed in a polymethylmethacrylate (PMMA) matrix. The experiments were conducted at room temperature. The complex nature of the recorded ESR spectra could be attributed to the superposition of the rotational diffusion component of TEMPO (or TEMPOL) in the nanospace of the PMMA matrix with the rigid-limit component. A single component of the rigid-limit was observed for 2-*X*-NN and 4-*Y*-PhBzNN radicals dispersed in the PMMA matrix. The isotropic components of *g* and hyperfine (*A*) tensor, estimated by analyzing the solution spectra, were used to determine the *g* and *A* components of 4-*Y*-PhBzNN. Only the rotational diffusion component was observed for the 2-*Z*-IN radical. These results demonstrated that the PMMA matrix contains cylindrical nanospaces. Various radicals other than TEMPO derivatives could be used in the ESR spin probe technique as probe molecules for determining the structures, sizes, and shapes of the nanospaces.

ESR spin probe technique using other than TEMPO derivatives



1. INTRODUCTION

The microscopic structure of a material can be revealed by using the characteristic atoms and molecules present in the material. Various magnetic resonance spectroscopic techniques are used to study the nuclear (such as ¹H and ¹³C) spins and the electron spins of unpaired electrons. Studies on the spin states of the nuclei and electrons in atoms or molecules can potentially help in revealing the microscopic structure of the matrices. The nuclear magnetic resonance (NMR) spectroscopy technique is used to study atoms with nonzero nuclear spin quantum numbers and nonradical molecules. Small and structurally simple molecules that can be used as probes are also studied using this technique.^{1–6} The electron spin resonance (ESR) spectroscopy is a powerful technique that can be used for the detection of organic radicals confined in the nanospaces of the material and nitroxide (NO) groups bonded to the material. The temperature dependence of the molecular dynamics of the confined radicals or NO moieties in the nanospace is studied to gain information on the structures, sizes, and shapes of the nanospaces present in porous materials,^{7–14} crystals,¹⁵ polymers,¹⁶ liquid crystals,¹⁷ supercooled bulk water,¹⁸ biological membranes,^{19,20} and proteins^{21–23} using the ESR spin probe technique. The dynamics of the moieties bearing the unpaired electrons are influenced by the structures or shapes of the nanospaces. The values of the *g* tensor and the hyperfine interaction (*A*) tensor of the unpaired electron are determined by analyzing the dynamics of the moieties bearing the unpaired electrons. The ESR spin

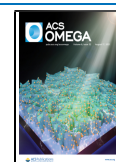
probe techniques can be divided into two categories: (i) the spin-label method executed by functionalizing the NO groups in the material^{9,14,19,21,23} and (ii) the method where the free radicals such as 4-substituted 2,2,6,6-tetramethyl-1-piperidinyloxy (4-*R*-TEMPO; 1: TEMPO (*R* = H) and 2: 4-hydroxy-TEMPO (TEMPOL; *R* = OH); Figure 1a) are physically adsorbed in the confined spaces.^{7,8,10–13,16,17,20,22}

In the past decade, the ESR spin probe technique has been used to study the organic 1D nanochannels of 2,4,6-tris (4-chlorophenoxy)-1,3,5-triazine and (*o*-phenylenedioxy)-cyclotriphosphazene crystals using 2-substituted nitronylnitroxide (2-*X*-NN, 3–5, Figure 1b).^{24,25} Nitronylnitroxide (NN) radicals are common organic radicals. Several radicals belonging to this group of radicals behave as organic magnets at low temperatures.^{26,27} Various NN radicals are present in the ligands in magnetic metal complexes^{28–30} and metal–organic frameworks (MOFs).³¹ Studies on the 2-*X*-NN radical present in frozen organic matrices, cement, and porous organic films have been rarely conducted using the ESR spectroscopy.^{32–34}

Received: April 23, 2021

Accepted: July 16, 2021

Published: August 4, 2021



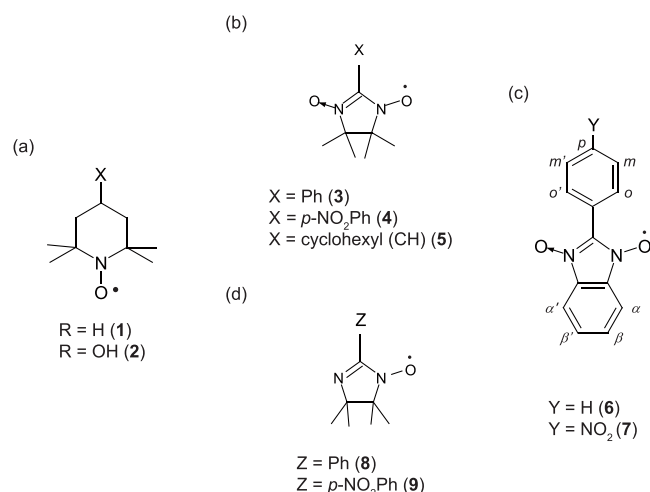


Figure 1. Chemical structures of guest radicals used in this study: (a) 4-R-TEMPO (1, 2), (b) 2-X-NN (3–5), (c) 4-Y-PhBzNN (6, 7), and (d) 2-Z-IN (8, 9).

The 4-substituted phenylbenzotrioxyl nitroxide (4-*Y*-PhBzNN, 6 and 7, in Figure 1c) radicals are structurally similar to NN radicals.^{35,36} To date, the ESR spectra of 4-*Y*-PhBzNN have only been recorded in the solution state. The complex nature of the ESR spectra, recorded with a solution of 4-*Y*-PhBzNN, can be attributed to the superhyperfine interactions (arising from the protons in the bicyclic structure containing the O—N—C—N—O moiety (α - or β -position (Figure 1c)); phenyl ring at the 2-position of the benzotrioxyl nitroxide (BzNN) group (*o*- or *m*-position (Figure 1c)); *p*-position when *Y* = H (Figure 1c)). The ESR spectra of the 2-*X*-NN radicals are less complex than the ESR spectra of the 4-*Y*-PhBzNN radicals. The isotropic values of the *g* and *A* tensors of these radicals have been reported.^{35,36} The *g* and *A* tensor components of the BzNN radicals should be examined in more detail in the dispersed state to gain insight into the nature of the 4-*Y*-PhBzNN radicals that can be potentially used as spin probes in the ESR spin probe technique. Details of the ESR spectra of phenyliminonitroxide (PhIN (8); *Z* = H; (Figure 1d)) present in organic matrices and 1D nanochannels have also been reported.^{25,33} The use of these radicals can help identify suitable probe radicals for further studies. The structures and shapes of the matrices, and the interactions between the matrices and guest radicals should be taken into consideration while selecting the suitable radicals for the studies.

Herein, several 2-*X*-NN (*X* = Ph (3), *p*-NO₂Ph (4), or cyclohexyl (CH; 5)), 4-*Y*-PhBzNN (*Y* = Ph (6) or NO₂ (7)), and iminonitroxide (IN) radicals substituted at the 2-position of the IN group (2-*Z*-IN, *Z* = Ph (8) or *p*-NO₂Ph (9); Figure 1d)^{33,37} dispersed in polymethylmethacrylate (poly(methyl 2-methylpropenoate); PMMA)^{38–47} matrices have been reported. The ESR spectra of these species were recorded. This is a rare case where the ESR spin probe technique was used to study the samples using non-TEMPO derivatives. PMMA is a transparent polymer that is often used as a lightweight alternative to glass.³⁸ It is also used as a casting resin during the preparation of dental prostheses.³⁹ PMMA contains cavities of varying sizes (large and small). The sizes of the cavities are influenced by the degrees of polymerization. The tacticity of the polymers and the synthetic method followed also influence the cavity sizes.^{40–42} Unpaired

electrons in PMMA can be produced via a numerous pathways. The process of mechanical fracture of PMMA,⁴¹ methods used to generate gamma-rays for sample irradiation,^{43,44} the spin-label method for the functionalization of PMMA,⁴⁵ and the method reported herein can be used to generate unpaired electrons. The spin probe technique can be used to study the adsorption and dispersion of the molecules containing unpaired electrons.^{47,48} The principal values of the *g* and *A* tensors of the organic radicals (other than TEMPO derivatives) dispersed in the PMMA matrices can be potentially used in the future for the further development of the field. These studies can potentially help expand the field of application of the ESR spin probe technique.

2. MATERIALS AND METHODS

2.1. Chemicals. PMMA (average molecular weight = 15,000) was purchased from Kanto Chemical Co. Ltd. Radicals 1–4 were purchased from Tokyo Chemical Industry Co. Ltd. Radicals 5–9 were synthesized following previously reported protocols.^{37,49,50} All the chemicals were used without further purification.

2.2. Sample Preparation. Radicals 1–9 were dispersed in PMMA. Radical 3 (0.2 mg) and PMMA (150 mg) were dissolved in CHCl₃ (10 mL). Following this, the solution was evaporated to dryness. The product was obtained as a transparent solid on the walls and the bottom of the beaker. The transparent solid was fractured using a microspatula to obtain the product in the form of a powder. A similar procedure was followed for preparing the samples in the presence of other radicals. The samples were stable for at least 6 months.

2.3. Instrumentation. ESR spectra were recorded at room temperature using an X-band spectrometer (JES-FA300 or RE-1X, Jeol) equipped with a TE₀₁₁ cylindrical cavity resonator. The powdered specimen (2–3 mg) was packed in a commercial ESR tube (quartz glass; length: 270 mm; o.d.: 5 mm). Following this, the tube was sealed under an atmosphere of He for prolonged storage, and future experiments were conducted under conditions of low temperature (pressure: 4 kPa). The benzene solution of the radicals (10⁵ mol L⁻¹) was poured into an ESR tube. The X-band (e.g., 9.07 GHz) microwave power was set in the range of 0.001–1 mW under nonsaturated conditions. The magnetic field range and field-sweep rate were set at 323 ± 15 mT and 30 mT/8 min, respectively. A field modulation of 100 kHz with an amplitude of 0.1 mT was used for the studies. The spin concentration was determined by comparing the double integral of the cw-ESR spectra of the weighed samples with that of the TEMPO standard solution. The signal intensity of a manganese standard was used as the reference. The experiments were carried out under conditions of a constant cavity loading. The estimated error was 30%.

The thermogravimetric-differential thermal analysis (TG-DTA) technique (thermogravimetric apparatus; TG-DTA8122, Rigaku Corp.) was used to study the PMMA matrix in the absence of dispersed radicals. The TG-DTA technique was also used to study the PMMA samples in the presence of small amounts of 1–4. Approximately 10 mg of the powdered specimen was placed in an Al sample pan. The sample was heated from room temperature to 500 °C at a rate of 10 °C min⁻¹ under an atmosphere of N₂. Powder Al₂O₃ was used as the reference. The endothermic peaks observed in the DTA curve in the temperature range of 90–110 °C (for the

PMMA sample) in the absence or presence of dispersed radicals correspond to the glass-to-liquid transition temperature (T_g ; Figures S1–S4). The T_g values were different from the previously reported values. The difference can be attributed to the difference in the average molecular weight of PMMA (average molecular weight = 94,000 in the previous study).⁵¹ A weight loss of 25% was observed in the PMMA sample in the absence of dispersed radicals, whereas a loss of 15–22% was observed in the presence of the dispersed radicals. The weight loss was higher than that observed for the powder PMMA samples, which did not dissolve in CHCl_3 (6%). It was believed that the solvent CHCl_3 molecules in the PMMA matrix were responsible for the weight loss. Positron annihilation lifetime spectroscopy (PALS) was conducted to determine the average diameter of the free volume in the PMMA matrix (average molecular weight = 94,000).⁵¹ The value was estimated to be approximately 0.6 nm at room temperature. The included CHCl_3 molecules remained confined in this space. The desorption temperature of the PMMA sample in the presence of dispersed radicals was higher than that in the absence of a small amount of the radical (Figures S1–S4). The hindrance to the inclusion/desorption of the solvent molecules can be attributed to the dispersed radicals (Section 3.1–4). The endothermic peaks corresponding to the radicals on the surface of the PMMA powder were not observed in the profiles recorded using the DTA technique (Section 3.1).

Various core functions present in the EasySpin program package^{52,53} (version 5.2.30, ETH Zürich) (such as Garlic (for solution spectra), Pepper (for solid-state spectra), and Chili (for anisotropic slow-motion cw-ESR spectra)) were used to simulate the spectra of radicals 1–9 dispersed in PMMA. A personal computer (PC; RAM: >8 GB) was used for running the calculations to analyze the data (obtained for radicals 8 and 9, in particular) using Chili (Section 3.4). The "Allocation" function of Opt should be set to "Opt.Allocation = [4e7 2e5]" during data analysis.^{52,53}

2.4. Procedure to Obtain the Rigid-Limit ESR Spectra of the Radicals Dispersed in PMMA. The Hamiltonian functions reported in the literature were used to describe the free radicals dispersed in the organic matrices and 1D nanochannels.^{24,25,52–55} Previously reported calculation methods were followed to describe the system where PMMA was used as the organic matrix. NO, 2-X-NN, 4-Y-PhBzNN, and 2-Z-IN radicals in the matrices were characterized as follows using the spin Hamiltonian:

$$\begin{aligned} \hat{H} = & \beta_e \mathbf{B} \cdot \mathbf{g} \cdot \hat{S} + \hat{S} \cdot \sum_{i=1,2} \mathbf{A}(\text{N}_i) \cdot \hat{I} \\ & + \hat{S} \cdot \sum_{j=\alpha, \alpha', \beta, \beta', o, o', m, m', p} \mathbf{A}(\text{H}_j) \cdot \hat{I} + \beta_n \cdot \mathbf{B} \cdot \sum_{i=1,2} \mathbf{g}_n(\text{N}_i) \cdot \hat{I} \\ & + \beta_n \cdot \mathbf{B} \cdot \sum_{j=\alpha, \alpha', \beta, \beta', o, o', m, m', p} \mathbf{g}_n(\text{H}_j) \cdot \hat{I} \end{aligned} \quad (1)$$

where β_e , \mathbf{B} , \mathbf{g} , $\mathbf{A}(\text{N}_i)$, $\mathbf{A}(\text{H}_j)$, β_n , $\mathbf{g}_n(\text{N}_i)$, $\mathbf{g}_n(\text{H}_j)$, \hat{S} , and \hat{I} denote the Bohr magneton; laboratory magnetic flux density vector; electron spin \mathbf{g} tensor; hyperfine tensor for the i th ^{14}N nucleus of the NO, 2-X-NN, 4-Y-PhBzNN, and 2-Z-IN radicals ($i = 1$ or 2); superhyperfine tensor of j th ^1H nucleus of 4-Y-PhBzNN ($j = \alpha, \beta, o, m, p$; the protons at α and α' , β and β' , o and o' , or m and m' are equivalent due to molecular symmetry; Figure 1c); nuclear magneton; nuclear spin \mathbf{g} tensor of the i th ^{14}N

nucleus of the NO, 2-X-NN, 4-Y-PhBzNN, and 2-Z-IN radicals; nuclear spin \mathbf{g} tensor of the j th ^1H nucleus of 4-Y-PhBzNN; electron spin operator; and nuclear spin operator, respectively. A number of factors can be attributed to molecular symmetry ($g_{\text{iso}} = (1/3)(g_{xx} + g_{yy} + g_{zz})$ and $A_{\text{iso}} = (1/3)(A_{xx} + A_{yy} + A_{zz})$): $\mathbf{g}(\text{N}_1) = \mathbf{g}(\text{N}_2)$ (that is, $(g(\text{N}_1))_{\text{iso}} = (g(\text{N}_2))_{\text{iso}}$) and $\mathbf{A}(\text{N}_1) = \mathbf{A}(\text{N}_2)$ (that is, $(A(\text{N}_1))_{\text{iso}} = (A(\text{N}_2))_{\text{iso}}$) for 2-X-NN and 4-Y-PhBzNN; $\mathbf{g}(\text{H}_j) = \mathbf{g}(\text{H}_j')$ (that is, $(g(\text{H}_j))_{\text{iso}} = (g(\text{H}_j'))_{\text{iso}}$) and $\mathbf{A}(\text{H}_j) = \mathbf{A}(\text{H}_j')$ (that is, $(A(\text{H}_j))_{\text{iso}} = (A(\text{H}_j'))_{\text{iso}}$) for 4-Y-PhBzNN when $j = \alpha, \beta, o$, or m (Figure 1c)).

The matrix diagonalization method was used as the default method of spectral simulation when the Pepper core function in the EasySpin program package was used for data analysis.^{52,53} For systems containing several nuclei (such as the 4-Y-PhBzNN radical), this process of calculation can be significantly time-consuming. The first- and second-order perturbation theory (integrated into Pepper) can be used to analyze the data at a faster rate. The appropriate simulation option that can be potentially used in EasySpin is the "Opt.Method". The rate of simulation increased the manifold when the second-order perturbation theory (Opt.Method = "perturb2") was used for carrying out the calculations. However, less accurate results were obtained.⁵³

The principal axes of the \mathbf{g} tensor of the NO, 2-X-NN, and 2-Z-IN radicals were defined following previous reports.^{24,25,32,54,55} The \mathbf{g} tensor corresponding to the 4-Y-PhBzNN radical was then determined. The unpaired electron present in the BzNN group was present in the π orbital. The lowest component of the \mathbf{g} tensor should be observed perpendicular to the molecular plane of the BzNN group, that is, along the principal z axis. It should be approximately 2.0023.^{24,32,55} As $g_{xx} > g_{yy} > g_{zz}$ for the 4-Y-PhBzNN radical, the intensity of the g_{xx} component is observed at the region of the lowest magnetic field.

The $\mathbf{A}(\text{N}_i)$ tensor (NO, 2-X-NN, and 2-Z-IN radicals) was defined following previously reported protocols.^{24,25,32,54,55} The $\mathbf{A}(\text{N}_i)$ tensor corresponding to the 4-Y-PhBzNN radical was determined following the protocol used to determine the $\mathbf{A}(\text{N}_i)$ tensor corresponding to the 2-X-NN radical. Unpaired electrons of 4-Y-PhBzNN occupy the π orbital ($2p_z$ orbitals of the nitrogen atoms). The spin density corresponding to the 4-Y-PhBzNN radical was significantly high, and the maximum value was recorded for the $A_{zz}(\text{N}_1)$ ($= A_{zz}(\text{N}_2)$) component. The values of $A_{xx}(\text{N}_1)$ and $A_{yy}(\text{N}_1)$ ($= A_{xx}(\text{N}_2)$ and $A_{yy}(\text{N}_2)$; 4-Y-PhBzNN radicals) should be potentially less than the value of $A_{zz}(\text{N}_1)$. Therefore, the $\mathbf{A}(\text{N}_i)$ tensor corresponding to the 4-Y-PhBzNN radical is anisotropic. For the $\mathbf{A}(\text{H}_j)$ tensors corresponding to the 4-Y-PhBzNN radicals, the unpaired electron occupies the s orbital of the hydrogen atom (present in the 4-Y-PhBzNN group). Therefore, the spin density of $A_{zz}(\text{H}_j)$ corresponding to the 4-Y-PhBzNN radicals is similar to the spin densities of $A_{xx}(\text{H}_j)$ (Section 3.3).

The rigid-limit ESR spectra of the 2-X-NN and 2-Z-IN radicals have been previously reported.^{24,25,55} The solid-state ESR spectra of the 4-Y-PhBzNN radical were broader and more complex than those of the 2-X-NN radicals (Sections 3.2 and 3.3). The characteristics of the profiles can be attributed to the superhyperfine pattern. The superhyperfine patterns of the 4-Y-PhBzNN radicals associated with the hydrogen atoms at α (or α'), β (or β'), o (or o'), m (or m'), and/or p -position further split the hyperfine interaction lines ($A_{zz}(\text{N}_i) \approx 10A_{kk}(\text{H}_j)$ ($k = x, y, \text{ or } z$)) associated with the equivalent

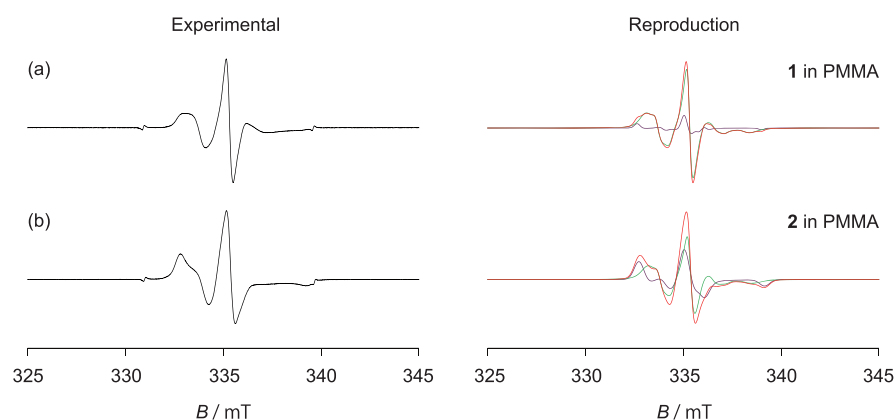


Figure 2. ESR spectra for (a) **1** (TEMPO; Figure 1a) and (b) **2** (TEMPOL; Figure 1a) dispersed in PMMA (black; left). The red-colored spectra (right) represent the reproduced spectra. The spectra were recorded at room temperature. Green and purple components (right) indicate rotational diffusion and rigid-limit components, respectively.

nitrogen atoms present in the 4-Y-PhBzNN radicals (Figure 1c). The hydrogen at the *p*-position was considered only when *Y* = H. If the molecular motions of the 4-Y-PhBzNN radicals dispersed in PMMA are assumed to be frozen, the solid-state ESR spectra recorded for the radicals can be reproduced using the principal values of the *g* and *A* tensors of the unpaired electrons, and the line width parameters and signal amplitudes.^{24,25,55} The *zz* components of the *g* and *A*(*N*₁) tensors of the 4-Y-PhBzNN radicals were estimated by visually inspecting the ESR spectra (*A*(*N*₁) is equal to *A*(*N*₂) for the 2-X-NN and 4-Y-PhBzNN radicals). It was difficult to guess the values of *g*_{*xx*}, *g*_{*yy*}, *A*_{*xx*}(*N*₁), *A*_{*yy*}(*N*₁), and *A*(*H*_{*j*}) from the solid-state ESR spectra for the 4-Y-PhBzNN radicals. The initial components of the principal axes of the *A*(*H*_{*j*}) tensors corresponding to the 4-Y-PhBzNN radicals were taken as *A*_{*xx*}(*H*_{*j*}) = *A*_{*yy*}(*H*_{*j*}) = *A*_{*zz*}(*H*_{*j*}) = (*A*(*H*_{*j*}))_{iso} estimated from the solution-state ESR spectra of the 4-Y-PhBzNN radicals using the Garlic core function in EasySpin. The final values of each component of the *g* and *A* tensors of the 4-Y-PhBzNN radical were estimated using the step-by-step variation technique. The variations in the *g* and *A* tensor components, line width parameters, and signal amplitudes were considered to minimize the sum of the squared differences (differences between the data obtained from the experimental and simulated spectra).

Previously reported protocols (used to determine the rotational axes of the radicals) were followed to reproduce the spectra in cases where all or some of the radicals in the matrices undergo molecular motion (**1**, **2**, and 2-Z-IN radicals dispersed in PMMA have been considered here).^{24,25,55} The rotational axes of the radicals dispersed in PMMA were defined by the polar and azimuthal angles (θ and ϕ , respectively) relative to the principal axis of the *g* tensor of each radical.^{24,25,54,55} Although four possible rotational axes were defined within the domains defined by $0 \leq \theta \leq \pi$ and $0 \leq \phi \leq 2\pi$, only the θ_0 and ϕ_0 values have been reported in the following section. The anisotropic rotational motion of each radical dispersed in PMMA can be potentially described by a Markov process (when a molecule undergoes numerous collisions accompanied by small and random angular reorientations).⁵⁶

The line shape is expressed by a Voigt function, which is defined by the Gaussian broadening (convolution) of a Lorentzian line.^{52,53,57} We have considered the full width at half-maximum (FWHM) as the line width parameter. The

anisotropic rotational diffusion in the nanospace was determined following the protocol outlined in previous reports, which reported the results obtained by studying the NO and IN radicals.^{25,52,53}

3. RESULTS AND DISCUSSION

3.1. ESR Spectra of TEMPO and TEMPOL Radicals Dispersed in PMMA Matrices. Figure 2a,b shows the ESR spectra recorded at room temperature with **1** (TEMPO; Figure 1a) and **2** (TEMPOL; Figure 1a) dispersed in PMMA. The results were reproduced as shown in Figure 2a,b. The maximum peak height was used to normalize both spectra (the same procedure was followed to normalize other spectra). The reproduced spectra could be obtained by superposing the rotational diffusion (green, Figure S5) and rigid-limit components (purple) of the dispersed NO radical. The following fractions were reported: 87 and 13% for **1** and 48 and 52% for **2**, respectively. These results revealed that a fraction of **1** (or **2**) dispersed in the PMMA matrix underwent anisotropic rotational diffusion in the nanospaces formed by folded or entangled polymer chains at room temperature. The origin of the rigid-limit component cannot be attributed to the radicals on the surface of PMMA (Section 2.3). The results indicated the presence of at least two types of nanospaces: (1) a cylindrical nanospace with a diameter of approximately 1 nm in consideration of the van der Waals volume of **1** (or **2**) (here, radical **1** (or **2**) can undergo rotational diffusion) and (2) a nanospace with a comparatively smaller diameter where the molecular motion (in the ESR time scale) of the dispersed **1** (or **2**) radical is restricted. The absence of molecular motion can be attributed to the influence of the folded or entangled polymer chains or the intermolecular interactions between the radicals and the PMMA chains. The PALS technique was previously used to report the existence of a space with an average diameter of 0.6 nm in the PMMA (average molecular weight = 94,000) at room temperature.⁵¹ The rigid-limit radicals of **1** (or **2**) present in the vicinity of the small space can potentially disturb the inclusion/desorption of the solvent molecules into/from PMMA. As the rotational diffusion of **1** (or **2**) is not isotropic but anisotropic, the probing radicals are expected to be present in the naturally existing space in the PMMA matrix and not in the space templated around the radical (because **1** (or **2**) is approximately spherical).

Table 1. *g* and *a* Tensor Components of **1** and **2** in Various Matrices^a

radicals	matrices	g_{xx}	g_{yy}	g_{zz}	A_{xx}/mT	A_{yy}/mT	A_{zz}/mT
1	grassy toluene ^b	2.0098	2.0062	2.0022	0.6	0.7	3.45
	TPP ^c	2.0100	2.0070	2.0024	0.60	0.55	3.35
	CLPOT ^d	2.0102	2.0062	2.0023	0.73	0.60	3.35
	PMMA (this study)	2.0091	2.0080	2.0044	1.09	0.50	3.18
2	TPP ^c	2.0092	2.0061	2.0026	0.83	0.30	3.33
	CLPOT ^d	2.0098	2.0062	2.0021	0.73	0.50	3.35
	TEMP-OH ^f	2.0099	2.0061	2.0024	0.53	0.70	3.50
	PMMA (this study)	2.0095	2.0070	2.0035	0.87	0.62	3.20

^aSpacer molecules in the case of footnotes c–e were abbreviated. ^bRef 58. From 20 to 70 K. ^cRef 59. At 112 K. ^dRef 60. At 55 K. ^eRef 61. ^fRef 62. At room temperature. TEMP-OH = 4-hydroxy-2,2,6,6-tetramethylpiperidine.

The spectra depicted in Figure 2a,b were reproduced using the *g* and *A* tensor components (Table 1; the rigid-limit components of the dispersed radical **1** (or **2**)). The g_{zz} values corresponding to radical **1** (or **2**) dispersed in PMMA shifted to the high *g*-value region (low field side). These values were higher than the g_{zz} values previously reported for **1** (or **2**) dispersed in various matrices.^{55,58–62} These results indicated that the PMMA chains were located close to radical **1** (or **2**). This potentially leads to the generation of the interactions between the PMMA chains (e.g., the π electrons present in the C=O groups in the PMMA chains) and the unpaired electron on the NO group of the radicals.

The rotational diffusion components determined from the ESR spectra (Figure 2a,b) were simulated following a model used to determine the anisotropic rotational diffusion of dispersed NO radicals. The motion was observed in the slow-motion regime (relative to the ESR time scale; $10^{-6} \text{ s} > \tau_R > 10^{-9} \text{ s}$). It was assumed that rotational diffusion was achieved along an axis tilted at an angle $((\theta, \phi) = (49^\circ, 51^\circ)$ for **1** and $(\theta, \phi) = (47^\circ, 58^\circ)$ for **2**; relative to the principal system of the *g* tensor using appropriate line width components). These results indicated that the θ and ϕ values recorded for the rotational diffusion of the TEMPO (or TEMPOL) radicals dispersed in the PMMA matrix were different than the average θ and ϕ recorded with several 4-substituted TEMPO radicals dispersed in the nanochannels of 2,4,6-tris(4-chlorophenoxy)-1,3,5-triazine (CLPOT) $((\theta, \phi) \approx (63^\circ, 38^\circ))$.⁵⁵ The rotational diffusion correlation time (τ_R) corresponding to **1** was similar to that corresponding to **2** (in PMMA). The values were estimated to be 4.4×10^{-8} and $4.6 \times 10^{-8} \text{ s}$, respectively. Therefore, the dynamics of **1** in PMMA were similar to the dynamics of **2** in PMMA. These indicated that the substituents at the 4-position of TEMPO did not influence the dynamics of the radical. These τ_R values were compared with the τ_R values of the 4-substituted TEMPO in CLPOT at temperatures below 250 K and the τ_R values of the 1D nanochannels of (*o*-phenylenedioxy)cyclotriphosphazene (TPP).^{59,60} The walls of CLPOT or TPP were formed by the π electrons of the phenyl ring.^{63,64} The strength of the interaction between the dispersed **1** (or **2**) radicals and the PMMA matrices can potentially be larger than the strength of the interaction between the dispersed **1** (or **2**) and the organic 1D nanochannels (exception: **2** in TPP).^{59–61} The extent of steric hindrance faced during rotational diffusion was more when radical **1** (or **2**) was dispersed in PMMA than the extent of steric hindrance faced during rotational diffusion when radical **1** (or **2**) was dispersed in organic 1D nanochannels.

3.2. ESR Spectra of 2-X-NN Radicals Dispersed in PMMA Matrix. Figure 3a–c shows the ESR spectra recorded

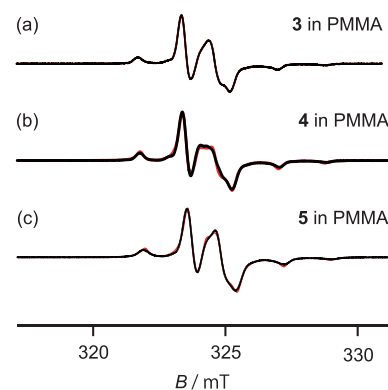


Figure 3. ESR spectra of 2-X-NN (*X* = (a) Ph (**3**), (b) *p*-NO₂Ph (**4**), or (c) CH (**5**); Figure 1b) dispersed in PMMA and the reproduced spectra (black and red). The spectra were recorded at room temperature.

for 2-X-NN (*X* = Ph (**3**), *p*-NO₂Ph (**4**), or CH (**5**); Figure 1b) dispersed in PMMA at room temperature. The reproduced spectra were also recorded at room temperature. The spectra could be well reproduced based on a rigid-limit powder pattern of a rigid NN radical dispersed in the matrix.^{24,25,55} The spectra obtained for the 2-X-NN radical dispersed in the PMMA matrix (Figure 3a–c) were simulated using the *g* and *A* tensor components (Table 2). The results agreed well with the results obtained by studying 2-X-NN dispersed in various matrices.^{24,25,32,33,55} The typical spectra of the dispersed NN radicals were recorded (Figure 3). It was confirmed that these NN radicals were adequately dispersed in the PMMA matrix. The interactions between the PMMA matrix and dispersed radicals (**3**–**5**) are ignored. The *g* and *A* tensor components of **5** were similar to those of **3** or **4**, indicating that the extent of spin delocalization into the phenyl ring from the NN group was small. The molecular motion of the NN radicals was potentially hindered and restricted by the folded or entangled PMMA chains. This potentially led to the confinement of the NN radicals in the PMMA matrix (approximately cylindrical; Section 3.1) nanospace with a diameter of approximately 1 nm. This can be attributed to the steric hindrance exerted by the PMMA chains on the NO moieties present in the NN group (Section 3.4). As the inclusion/desorption of CHCl₃ in the PMMA matrix is influenced, some space may be present near the space observed using the PALS technique (Section 3.1).⁵¹

As previously reported, when compound **3** (or **4**) was dispersed in the CLPOT nanochannels, the rotational diffusion of the NN radicals was observed at temperatures higher than room temperature. This could be attributed to the increased number of host–guest interactions and significantly high

Table 2. Tensor Components of g and A of 2- X -NN ($X = \text{Ph}$ (3), $p\text{-NO}_2\text{Ph}$ (4), or CH (5)) Radicals in Various Matrices^a

radicals	matrices	g_{xx}	g_{yy}	g_{zz}	$A_{xx}(\text{N})/\text{mT}$	$A_{yy}(\text{N})/\text{mT}$	$A_{zz}(\text{N})/\text{mT}$
3	Duco cement ^b	2.0127	2.0068	2.0028	0.52	0.52	1.80
	grassy toluene ^c	2.0100	2.0065	2.0021			1.86
	CLPOT ^d	2.0118	2.0075	2.0031	0.34	0.12	1.74
	TPP ^e	2.0107	2.0086	2.0031	0.01	0.01	2.13
	PMMA (this study)	2.0105	2.0072	2.0031	0.33	0.04	1.74
4	CLPOT ^d	2.0116	2.0076	2.0030	0.32	0.16	1.77
	PMMA (this study)	2.0111	2.0071	2.0031	0.23	0.19	1.74
5	PMMA (this study)	2.0105	2.0070	2.0030	0.34	0.01	1.75

^aSpacer molecules in the case of footnotes d and e were abbreviated. ^bRef 32. ^cRef 33. ^dRef 24. ^eRef 25. Co-inclusion with PhIN.

molecular moment of inertia.^{24,55} The rotational diffusion of the 2- X -NN radicals in the PMMA matrices could also be observed at elevated temperatures. However, at elevated temperatures, the PMMA matrix can potentially melt and undergo structural changes.

3.3. ESR Spectra of 4- Y -PhBzNN Radicals Dispersed in PMMA Matrix. Figure 4a,b shows the ESR spectra recorded

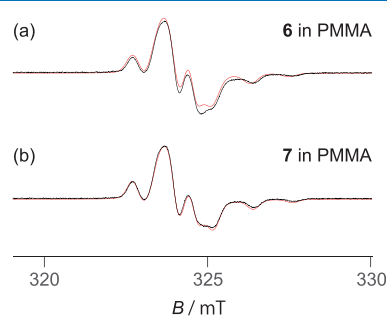


Figure 4. ESR spectra recorded for 4- Y -PhBzNN ((a) $X = \text{H}$ (6) or (b) NO_2 (7); Figure 1c) dispersed in PMMA (black) and reproduced spectra (red). The spectra were recorded at room temperature.

for 4- Y -PhBzNN ($Y = \text{H}$ (6) or NO_2 (7); Figure 1c) dispersed in PMMA (black) and the reproduced spectra. They could be reproduced on the basis of a rigid-limit powder pattern of the PhBzNN radical dispersed in a matrix. The superhyperfine coupling between the unpaired electron on the BzNN group and the hydrogen in 4- Y -PhBzNN (Figure 1c) led to the perturbation of the characteristic rigid-limit powder pattern exhibited by the PhBzNN radicals. The extent of perturbation was less in the case of the NN radicals (Section 2.4; Figures 3 and 4). These results revealed that the 4- Y -PhBzNN radicals were adequately dispersed in the PMMA matrix. The folded or entangled PMMA polymer chains restricted the molecular motion of 4- Y -PhBzNN. This can potentially lead to the confinement of the PhBzNN radicals in the (approximately cylindrical; Section 3.1) nanospaces (diameter: approximately 1 nm) present in the PMMA matrices. This can be attributed to the steric hindrance exerted by the PMMA chains on the 4- Y -PhBzNN radical, the extent of which is relatively larger than the extent of steric hindrance exerted on the 2- X -NN and 2- Z -IN radicals (Sections 3.2 and 3.4).

The spectrum recorded with 6 (or 7) dispersed in the PMMA matrix was simulated using the components of the g and A tensors (Table 3). The g_{iso} , $(A(\text{N}))_{\text{iso}}$, and $(A(\text{H}_j))_{\text{iso}}$ ($j = \alpha, \beta, o, m,$ and p) values for the radicals (Table 4) estimated from the solution-state ESR spectra of 6 (or 7) (Figure 5a,b, respectively; Garlic program in EasySpin (Section 2.4)) were used to determine the g and A component values (Section

Table 3. Tensor Components of g , A_{N} , and $A_{kk}(\text{H}_j)$ ($j = \alpha, \beta, o, m,$ and p ; $k = x, y,$ and z ; Figure 1c) of 4- Y -PhBzNN ($Y = \text{H}$ (6) or NO_2 (7)) Dispersed in PMMA

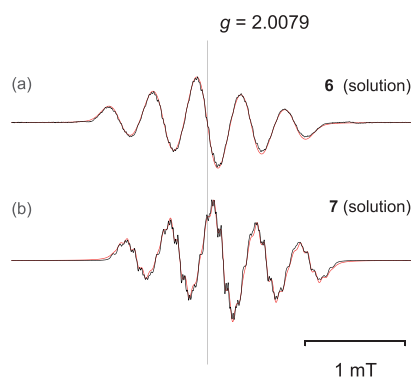
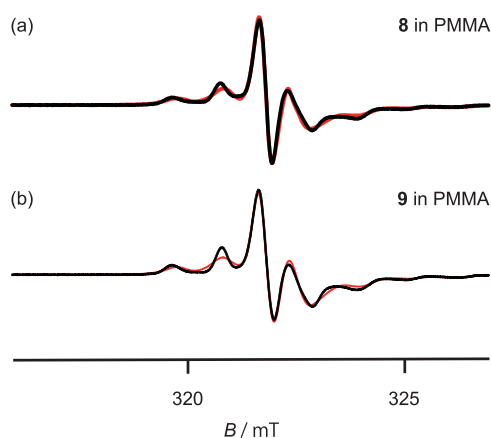
tensor components	states	
	6 in PMMA	7 in PMMA
g_{xx}	2.0121	2.0118
g_{yy}	2.0071	2.0068
g_{zz}	2.0032	2.0028
$A_{xx}(\text{N})/\text{mT}$	0.11	0.07
$A_{yy}(\text{N})/\text{mT}$	0.03	0.02
$A_{zz}(\text{N})/\text{mT}$	1.17	1.20
$A_{xx}(\text{H}_\alpha)/\text{mT}$	0.10	0.09
$A_{yy}(\text{H}_\alpha)/\text{mT}$	0.00	0.07
$A_{zz}(\text{H}_\alpha)/\text{mT}$	0.14	0.09
$A_{xx}(\text{H}_\beta)/\text{mT}$	0.11	0.09
$A_{yy}(\text{H}_\beta)/\text{mT}$	0.00	0.02
$A_{zz}(\text{H}_\beta)/\text{mT}$	0.09	0.09
$A_{xx}(\text{H}_o)/\text{mT}$	0.09	0.06
$A_{yy}(\text{H}_o)/\text{mT}$	0.00	0.05
$A_{zz}(\text{H}_o)/\text{mT}$	0.06	0.06
$A_{xx}(\text{H}_m)/\text{mT}$	0.05	0.01
$A_{yy}(\text{H}_m)/\text{mT}$	0.00	0.02
$A_{zz}(\text{H}_m)/\text{mT}$	0.03	0.01
$A_{xx}(\text{H}_p)/\text{mT}$	0.07	
$A_{yy}(\text{H}_p)/\text{mT}$	0.00	
$A_{zz}(\text{H}_p)/\text{mT}$	0.05	

2.4). The calculated g_{iso} , $(A(\text{N}))_{\text{iso}}$, and $(A(\text{H}_j))_{\text{iso}}$ values (estimated from the tensor components; Table 3) agreed well with the previously reported g_{iso} , $(A(\text{N}))_{\text{iso}}$, and $(A(\text{H}_j))_{\text{iso}}$ values calculated for 6 and other BzNN derivatives such as p -pyridinyl-BzNN.³⁵ The value of $A_{zz}(\text{N})$ corresponding to the 4- Y -PhBzNN radical was smaller than that of the 2- X -NN radical (Table 2). The value of $A_{xx}(\text{H}_j)$ was comparable to the value of $A_{zz}(\text{H}_j)$ and originated from the spin delocalization into the annulated aromatic moiety and the protons present in the aryl moiety in PhBzNN. The superhyperfine coupling between the unpaired electron and the protons in the aryl moiety in PhBzNN also influenced the values of the components.³⁵ The rotational diffusion of the 4- Y -PhBzNN radicals in the PMMA matrices can be potentially recorded at elevated temperatures, although the PMMA matrices can melt and undergo structural changes at elevated temperatures. The molecular shape (Figure 1d) of 4- Y -PhBzNN makes it a suitable spin probe molecule that can be used in two-dimensional nanospaces. The suitability can be attributed to the planarity of the structure.

3.4. ESR Spectra Recorded with 2- Z -IN Radicals Dispersed in PMMA Matrix. Figure 6a,b shows the ESR

Table 4. g_{iso} , $(A(\text{N}))_{\text{iso}}$ and $(A(\text{H}_j))_{\text{iso}}$ ($j = \alpha, \beta, o, m, \text{ or } p$; Figure 1c) for 6 and 7 under Various Conditions

state		g_{iso}	$(A(\text{N}))_{\text{iso}}/\text{mT}$	$(A(\text{H}_\alpha))_{\text{iso}}/\text{mT}$	$(A(\text{H}_\beta))_{\text{iso}}/\text{mT}$	$(A(\text{H}_o))_{\text{iso}}/\text{mT}$	$(A(\text{H}_m))_{\text{iso}}/\text{mT}$	$(A(\text{H}_p))_{\text{iso}}/\text{mT}$
6	benzene solution ^a	2.007	0.437	0.093	0.065	0.049	0.022	0.041
	benzene solution (this study)	2.0078	0.437	0.078	0.065	0.049	0.022	0.040
	the average of the principal axis components shown in Table 3 (this study)	2.0075	0.438	0.081	0.066	0.052	0.029	0.041
7	in benzene solution (this study)	2.0068	0.432	0.078	0.064	0.057	0.010	
	the average of the principal axis components shown in Table 3 (this study)	2.0072	0.434	0.083	0.067	0.058	0.012	
<i>p</i> -pyridinylBzNN ^a		2.0072	0.426	0.091	0.073	0.041	0.020	

^aRef 33.**Figure 5.** ESR spectra recorded for 4-Y-PhBzNN ((a) X = H (6) and (b) NO₂ (7); Figure 1c) dissolved in benzene (black) and reproduced spectra (red). The spectra were recorded at room temperature.**Figure 6.** ESR spectra recorded for 2-Z-IN ((a) Z = Ph (8) and (b) *p*-NO₂Ph (9); Figure 1d) dispersed in PMMA (black) and the reproduced spectra (red). The spectra were recorded at room temperature.

spectra recorded at room temperature with radicals 8 or 9 dispersed in PMMA and the reproduced spectra. The spectra could be reproduced on the basis of the rotational diffusion component of the dispersed IN radical (Figure S5).²⁵ The spectra recorded with 8 and 9 in the PMMA matrix (Figure 6a,b, respectively) were simulated using the g and A tensor components (Table 5). The values of the g and A tensors agreed well with the values reported previously for 8 and other IN derivatives (in various matrices; Table 5).^{25,33,55} These results revealed that most of the IN radicals in the PMMA matrix underwent anisotropic rotational diffusion in the cylindrical nanospaces described in Section 3.1 (diameter:

Table 5. Tensor Components of g , $a(\text{N}_1)$, and $a(\text{N}_2)$ Corresponding to Radicals 8 and 9 under Various Conditions

tensor components	states				
	8		9		
	in glassy toluene ^c	in TPP ^e	in PMMA (this study)	PMMA (this study)	PhIN derivative in glassy toluene ^c
g_{xx}	2.0093	2.0103	2.0098	2.0098	2.0098
g_{yy}	2.0060	2.0050	2.0067	2.0063	2.0059
g_{zz}	2.0022	2.0028	2.0023	2.0022	2.0023
$A_{xx}(\text{N}_1)/\text{mT}$		0.02	0.33	0.29	
$A_{yy}(\text{N}_1)/\text{mT}$		0.01	0.00	0.01	
$A_{zz}(\text{N}_1)/\text{mT}$	2.32	2.36	2.43	2.45	2.17
$A_{xx}(\text{N}_2)/\text{mT}$		0.01	0.08	0.06	
$A_{yy}(\text{N}_2)/\text{mT}$		0.02	0.00	0.00	
$A_{zz}(\text{N}_2)/\text{mT}$	1.28	1.16	1.18	1.15	1.14

^aRef 33. The methyl groups at the 4 and 4' positions were substituted with the phenyl and methoxy groups in the "PhIN derivative in glassy toluene". ^bRef 25.

approximately 1 nm) formed by folded or entangled polymer chains at room temperature. These results indicate that 8 (or 9) can be readily included in the cylindrical spaces in the PMMA matrix.

The rotational diffusion components estimated from the ESR spectra (Figure 6a,b) were simulated following a model used for simulating the anisotropic rotational diffusion of dispersed IN radicals (a slow-motion regime (relative to the ESR time scale); $10^{-6} \text{ s} > \tau_R > 10^{-9} \text{ s}$). It was assumed that rotational diffusion was achieved along a tilted axis ($(\theta, \phi) = (79^\circ, 90^\circ)$ for 8 and $(\theta, \phi) = (78^\circ, 90^\circ)$ for 9; relative to the principal system of the g tensor with appropriate line width components). These results indicated that the rotational diffusion of 8 and 9 dispersed in PMMA could be observed along the molecular long axis. The θ and ϕ values were comparable to the θ and ϕ values recorded for 8 dispersed in TPP nanochannels ($(\theta, \phi) \approx (90^\circ, 73^\circ)$). The τ_R values corresponding to 8 were similar to those corresponding to 9, dispersed in PMMA. The values were estimated to be $1.4 \times 10^{-7} \text{ s}$ for 8 and $1.5 \times 10^{-7} \text{ s}$ for 9. Therefore, the dynamics of 8 and 9 (in PMMA) were similar to each other. The substituent at the 4-position of the phenyl group present in the skeleton structure of radicals 8 and 9 did not influence the molecular dynamics. These τ_R values were compared with the τ_R values recorded for 8 in TPP 1D nanochannels at approximately 200 K.²⁵ These results can be attributed to the steric hindrance exerted by the PMMA chains on the NO

groups present in the IN and NN moieties (Section 3.2) and the strong interactions present between the dispersed 8 radical and the PMMA matrix or TPP nanochannels.

When 1 (or 2; Section 3.1) was the radical of choice, the complex spectra were reproduced using the rotational diffusion and rigid-limit components. The simple ESR spectra recorded with 8 and 9 dispersed in PMMA were reproduced using the rotational diffusion components. These results indicated that the nanospaces in the PMMA matrix could be studied using 8 (or 9) as the ESR spin probe. Suitable organic radicals (such as TEMPO derivatives, 2-Z-IN, 2-X-NN, and 4-Y-PhBzNN) can be potentially selected as probes to be used in the ESR spin probe technique. The choice of the radicals depends on the structure and shape of the nanospaces in the matrices. It also depends on the type and strength of the interactions present between the matrices and the guest radicals.

4. CONCLUSIONS

TEMPO derivatives and non-TEMPO radicals (such as 2-X-NN, 4-Y-PhBzNN, and 2-Z-IN) were dispersed in the PMMA matrices. The structures, sizes, and shapes of the nanospaces in the PMMA matrix were examined using the ESR spectroscopy technique. The spectra recorded with the TEMPO derivatives, dispersed in the PMMA matrix, were complex. The complex nature of the spectra could be attributed to the mixed rigid-limit and rotational diffusion state of the probe radicals. The spectra corresponding to 2-Z-IN were reproduced using the uniaxial rotational diffusion components. These results demonstrated that 2-Z-IN radicals could be potentially used as spin probes for studying the characteristics of PMMA. The sign of the molecular motion in 2-X-NN and 4-Y-PhBzNN (dispersed in PMMA) was not determined using ESR spectroscopy. This method could also be used to study the structures, sizes, and shapes of the nanospaces in the matrices of various organic polymers in the presence of 2-X-NN and 4-Y-PhBzNN radicals. These results revealed that the ESR spin probe technique could be used to study samples using non-TEMPO derivatives to study the chemical and biological structures of nanosized materials (such as nanosized cavities, polymers, membranes, and dental materials). The existence of the nanosized spaces containing the imino or nitronyl nitroxide groups has been reported in recent years.^{34,65,66} The results reported herein can be used to develop such novel systems. The radicals used may be introduced inside the preformed pores in the polymer samples by exposing in a sealed test tube to conditions of reduced pressure or penetrating in the radical solution. Further investigations on this topic are currently underway in our laboratory.

■ ASSOCIATED CONTENT

SI Supporting Information

The Supporting Information is available free of charge at <https://pubs.acs.org/doi/10.1021/acsomega.1c02170>.

TG-DTA curves of PMMA sample in the presence of small amounts of 1 (Figure S1); TG-DTA curves of PMMA sample in the presence of small amounts of 2 (Figure S2); TG-DTA curves of PMMA sample in the presence of small amounts of 3 (Figure S3); TG-DTA curves of PMMA sample in the presence of small amounts of 4 (Figure S4); typical spectral reproduction and the principal axes of the *g*-tensor of 4-R-TEMPO

and 2-Z-IN, and the direction of the rotation axis (Figure S5) (PDF)

■ AUTHOR INFORMATION

Corresponding Author

Hirokazu Kobayashi – Faculty of Arts and Sciences at Fujiyoshida, Showa University, Yamanashi 403-0005, Japan; orcid.org/0000-0002-8643-1500; Phone: +81-555-22-6625; Email: hirawk@cas.showa-u.ac.jp

Authors

Kento Akiniwa – Graduate School of Integrated Basic Sciences, College of Humanities and Sciences, Nihon University, Tokyo 156-8550, Japan

Fumiyasu Iwahori – Department of Chemistry, College of Humanities and Sciences, Nihon University, Tokyo 156-8550, Japan

Hidehiko Honda – Faculty of Arts and Sciences at Fujiyoshida, Showa University, Yamanashi 403-0005, Japan

Masato Yamamoto – Faculty of Arts and Sciences at Fujiyoshida, Showa University, Yamanashi 403-0005, Japan

Yuki Odanaka – Department of Pharmaceutical Sciences, Division of Bioanalytical Chemistry, Showa University, Tokyo 142-8555, Japan

Masahiro Inagaki – Faculty of Arts and Sciences at Fujiyoshida, Showa University, Yamanashi 403-0005, Japan

Complete contact information is available at: <https://pubs.acs.org/10.1021/acsomega.1c02170>

Funding

This work was partially supported by the Common Research Funding granted by Showa University (2017–2019 (17FY02)).

Notes

The authors declare no competing financial interest.

■ ACKNOWLEDGMENTS

This work was partially funded by the Common Research Funding granted by Showa University (2017–2019; 17FY02). The authors wish to thank Prof. S. Stoll, working at the University of Washington, for helping with the EasySpin calculations. We would like to thank Editage (www.editage.com) for English language editing.

■ REFERENCES

- (1) Perunicic, V. S.; Hill, C. D.; Hall, L. T.; Hollenberg, L. C. L. A Quantum Spin-Probe Molecular Microscope. *Nat. Commun.* **2016**, *7*, 12667.
- (2) Ramírez-Ruiz, J.; Boutin, S.; Garate, I. NMR in an Electric Field: A Bulk Probe of the Hidden Spin and Orbital Polarizations. *Phys. Rev. B: Condens. Matter Mater. Phys.* **2017**, *96*, 235201.
- (3) Carper, W. R.; Pflug, J. L.; Wilkes, J. S. Dual Spin Probe NMR Relaxation Studies of Ionic Structure in 1-Ethyl-3-methylimidazolium Chloride-AlCl₃ Molten Salts. *Inorg. Chim. Acta* **1992**, *202*, 89–93.
- (4) Ueda, T.; Yamatani, T.; Okumura, M. Dynamic Gate Opening of ZIF-8 for Bulky Molecule Adsorption as Studied by Vapor Adsorption Measurements and Computational Approach. *J. Phys. Chem. C* **2019**, *123*, 27542–27553.
- (5) Bezsonova, I.; Forman-Kay, J.; Prosser, R. S. Molecular Oxygen as a Paramagnetic NMR Probe of Protein Solvent Exposure and Topology. *Concepts Magn. Reson.* **2008**, *32A*, 239–253.
- (6) Kimura, A.; Yamauchi, Y.; Hodono, S.; Stewart, N. J.; Hosokawa, O.; Hagiwara, Y.; Imai, H.; Fujiwara, H. Treatment Response of Ethyl Pyruvate in a Mouse Model of Chronic Obstructive Pulmonary

Disease Studied by Hyperpolarized ^{129}Xe MRI. *Magn. Reson. Med.* **2017**, *78*, 721–729.

(7) Jayaraj, N.; Porel, M.; Ottaviani, M. F.; Maddipatla, M. V. S. N.; Modelli, A.; Da Silva, J. P.; Bhogala, B. R.; Captain, B.; Jockusch, S.; Turro, N. J.; Ramamurthy, V. Self Aggregation of Supramolecules of Nitroxides@Cucurbit[8]uril Revealed by EPR Spectra. *Langmuir* **2009**, *25*, 13820–13832.

(8) Soegiarto, A. C.; Yan, W.; Kent, A. D.; Ward, M. D. Regulating Low-Dimensional Magnetic Behavior of Organic Radicals in Crystalline Hydrogen-Bonded Host Frameworks. *J. Mater. Chem.* **2011**, *21*, 2204–2219.

(9) Rinkevicius, Z.; Frecuș, B.; Murugan, N. A.; Vahtras, O.; Kongsted, J.; Ågren, H. Encapsulation Influence on EPR Parameters of Spin-Labels: 2,2,6,6-Tetramethyl-4-methoxypiperidine-1-oxyl in Cucurbit[8]uril. *Adv. Funct. Mater.* **2012**, *8*, 257–263.

(10) Cowley, H. J.; Hayward, J. J.; Pratt, D. R.; Rawson, J. M. Inclusion Chemistry of a Thiazyl Radical in Zeolite-Y. *Dalton Trans.* **2014**, *43*, 1332–1337.

(11) Okazaki, M.; Anandan, S.; Seelan, S.; Nishida, M.; Toriyama, K. Spin-Probe ESR Study on the Entrapment of Organic Solutes by the Nanochannel of MCM-41 in Benzene. *Langmuir* **2007**, *23*, 1215–1222.

(12) Nikolayenko, V. I.; Barbour, L. J.; Arauzo, A.; Campo, J.; Rawson, J. M.; Haynes, D. A. Inclusion of a Dithiadiazolyl Radical in a Seemingly Non-Porous Solid. *Chem. Commun.* **2017**, *53*, 11310–11313.

(13) Poryvaev, A. S.; Sheveleva, A. M.; Kolokolov, D. I.; Stepanov, A. G.; Bagryanskaya, E. G.; Fedin, M. V. Mobility and Reactivity of 4-Substituted TEMPO Derivatives in Metal–Organic Framework MIL-53(Al). *J. Phys. Chem. C* **2016**, *120*, 10698–10704.

(14) Dzikovski, B.; Tipikin, D.; Livshits, V.; Earle, K.; Freed, J. Multifrequency ESR Study of Spin-Labeled Molecules in Inclusion Compounds with Cyclodextrins. *Phys. Chem. Chem. Phys.* **2009**, *11*, 6676–6688.

(15) Lukešová, M.; Zgardzinska, B.; Švajdenková, H.; Zaleski, R.; Charmas, B.; Bartoš, J. Spin Probe Dynamics in Relation to Free Volume in Crystalline Organics from ESR and PALS: N-Tridecane. *Phys. B* **2015**, *476*, 100–108.

(16) Albulnia, A. R.; D'Aniello, C.; Guerra, G.; Gatteschi, D.; Mannini, M.; Sorace, L. Ordering Magnetic Molecules Within Nanoporous Crystalline Polymers. *Chem. Mater.* **2009**, *21*, 4750–4752.

(17) Chmielewski, P.; Jezierski, A. ESR Study on Silver(II) Dithiocarbamate Complexes in Nematic Liquid Crystal. *Polyhedron* **1988**, *7*, 25–28.

(18) Banerjee, D.; Bhat, S. N.; Bhat, S. V.; Leporini, D. ESR Evidence for 2 Coexisting Liquid Phases in Deeply Supercooled Bulk Water. *Proc. Natl. Acad. Sci. U. S. A.* **2009**, *106*, 11448–11453.

(19) Sryyamina, V. N.; De Zotti, M.; Toniolo, C.; Formaggio, F.; Dzuba, S. A. Alamethicin Self-Assembling in Lipid Membranes: Concentration Dependence from Pulsed EPR of Spin Labels. *Phys. Chem. Chem. Phys.* **2018**, *20*, 3592–3601.

(20) Nakagawa, K. ESR Spin Probe Investigation of Chain Ordering of a Triglycerol Membrane. *Bull. Chem. Soc. Jpn.* **2004**, *77*, 269–273.

(21) Muok, A. R.; Chua, T. K.; Le, H.; Crane, B. R. Nucleotide Spin Labeling for ESR Spectroscopy of ATP-Binding Proteins. *Appl. Magn. Reson.* **2018**, *49*, 1385–1395.

(22) Kazmierczak, S. C.; Gurachevsky, A.; Matthes, G.; Muravsky, V. Electron Spin Resonance Spectroscopy of Serum Albumin: A Novel New Test for Cancer Diagnosis and Monitoring. *Clin. Chem.* **2006**, *52*, 2129–2134.

(23) Delannoy, S.; Urbatsch, I. L.; Tomblin, G.; Senior, A. E.; Vogel, P. D. Nucleotide Binding to the Multidrug Resistance P-Glycoprotein as Studied by ESR Spectroscopy. *Biochemistry* **2005**, *44*, 14010–14019.

(24) Kobayashi, H.; Morinaga, Y.; Fujimori, E.; Asaji, T. ESR Study of Molecular Orientation and Dynamics of Nitronyl Nitroxide Radicals in CLPOT 1D Nanochannels. *J. Phys. Chem. A* **2014**, *118*, 4907–4917.

(25) Kobayashi, H.; Mori, T.; Morinaga, Y.; Fujimori, E.; Akiniwa, K.; Iwahori, F. Electron Spin Resonance Study of Molecular Orientation and Dynamics of Phenyl Imino and Nitronyl Nitroxide Radicals in Organic 1D Nanochannels of Tris(*o*-phenylenedioxy)-cyclotriphosphazene. *J. Phys. Chem. A* **2018**, *122*, 5493–5502.

(26) Kinoshita, M.; Turek, P.; Tamura, M.; Nozawa, K.; Shiomi, D.; Nakazawa, Y.; Ishikawa, M.; Takahashi, M.; Awaga, K.; Inabe, T.; Maruyama, Y. An Organic Radical Ferromagnet. *Chem. Lett.* **1991**, *20*, 1225–1228.

(27) Amabilino, D. B.; Veciana, J. *Magnetism: Molecules to Materials*, (Miller, J. S.; Dillon, M., Ed.), part II, Molecule-Based Materials, Ch. 1, Nitroxide-Based Organic Magnets. Wiley-VCH Verlag GmbH & Co KGaA, Weinheim, Germany, 2003, 1–60.

(28) Meng, X.; Shi, W.; Cheng, P. Magnetism in One-Dimensional Metal–Nitronyl Nitroxide Radical System. *Coord. Chem. Rev.* **2019**, *378*, 134–150.

(29) Tichnell, C. R.; Shultz, D. A.; Popescu, C. V.; Sokirniy, I.; Boyle, P. D. Synthesis, Characterization, and Photophysical Studies of an Iron(III) Catecholate-Nitronyl Nitroxide Spin-Crossover Complex. *Inorg. Chem.* **2015**, *54*, 4466–4474.

(30) Vaz, M. G. F.; Cassaro, R. A.; Akpınar, H.; Schlueter, J. A.; Lahti, P. M.; Novak, M. A. A Cobalt Pyrenyl Nitronyl Nitroxide Single-Chain Magnet with High Coercivity and Record Blocking Temperature. *Eur. J. Chem.* **2014**, *20*, 5460–5467.

(31) Houard, F.; Evrard, Q.; Calvez, G.; Suffren, Y.; Daiguebonne, C.; Guillou, O.; Gendron, F.; Le Guennic, B.; Guizouarn, T.; Dorcet, V.; Mannini, M.; Bernot, K. Chiral Supramolecular Nanotubes of Single-Chain Magnets. *Angew. Chem. Int. Ed. Engl.* **2020**, *59*, 780–784.

(32) D'Anna, J. A.; Wharton, J. H. Electron Spin Resonance Spectra of α -Nitronyl Nitroxide Radicals; Solvent Effects; Nitrogen Hyperfine Tensor; *g* Anisotropy. *J. Chem. Phys.* **1970**, *53*, 4047–4052.

(33) Dikanov, S. A.; Gulin, V. I.; Tsvetkov, Y. D.; Grigor'ev, I. A. 2 mm Electron Paramagnetic Resonance Studies of the New Types of Imidazoline Nitroxide Radicals. *Faraday Trans.* **1990**, *86*, 3201–3205.

(34) Hui, P.; Chandrasekar, R. Shape-Defined and Shape-Shifting Paramagnetic Organic Nano/Microstructures Derived from a Doublet State Nitronyl Nitroxide Radical. *ChemPlusChem* **2012**, *77*, 1062–1065.

(35) Dooley, B. M.; Bowles, S. E.; Storr, T.; Frank, N. L. Synthesis of Neutral Spin-Delocalized Electron Acceptors for Multifunctional Materials. *Org. Lett.* **2007**, *9*, 4781–4783.

(36) Lahti, P. M.; Esat, B.; Liao, Y.; Serwinski, P.; Lan, J.; Walton, R. Heterospin Organic Molecules: Nitrene–Radical Linkages. *Polyhedron* **2001**, *20*, 1647–1652.

(37) Zhao, M.; Li, Z.; Peng, L.; Tang, Y. R.; Wang, C.; Zhang, Z.; Peng, S. Novel 1-Oxyl-2-substitutedphenyl-4,4,5,5-tetramethylimidazolines: Synthesis, Selectively Analgesic Action, and QSAR Analysis. *Bioorg. Med. Chem.* **2007**, *15*, 2815–2826.

(38) Yeh, S. L.; Zhu, C. Y.; Kuo, S. W. Transparent Heat-Resistant PMMA Copolymers for Packing Light-Emitting Diode Materials. *Polymer* **2015**, *7*, 1379–1388.

(39) Matsuo, H.; Suenaga, H.; Takahashi, M.; Suzuki, O.; Sasaki, K.; Takahashi, N. Deterioration of Polymethyl Methacrylate Dentures in the Oral Cavity. *Dent. Mater. J.* **2015**, *34*, 234–239.

(40) Kawauchi, T.; Kumaki, J.; Kitaura, A.; Okoshi, K.; Kusanagi, H.; Kobayashi, K.; Sugai, T.; Shinohara, H.; Yashima, E. Encapsulation of Fullerenes in a Helical PMMA Cavity Leading to a Robust Processable Complex with a Macromolecular Helicity Memory. *Angew. Chem. Int. Ed. Engl.* **2008**, *47*, 515–519.

(41) Kontturi, E.; Johansson, L. S.; Laine, J. Cellulose Decorated Cavities on Ultrathin Films of PMMA. *Soft Matter* **2009**, *5*, 1786–1788.

(42) Abderrahmane, C.; Migalska-Zalas, A.; Arof, A. K.; Sofiani, Z.; Sahrroui, B. Wide and Intense Emission Band in the Visible Area in CdSe Nanocrystals Dispersed in PMMA. *Nonlinear Opt. Quantum Opt.* **2015**, *47*, 73–83.

- (43) Kaptan, H. Y.; Tatar, L. An Electron Spin Resonance Study of Mechanical Fracture of Poly(Methyl Methacrylate). *J. Appl. Polym. Sci.* **1997**, *65*, 1161–1167.
- (44) Trihi, M.; Duroux, J. L.; Hyvernaud, M. J.; Bernard, M. Study of Free Radicals in Irradiated PMMA (Doped or Undoped) Using ESR Spectroscopy. *Appl. Radiat. Isot.* **1996**, *47*, 1561–1563.
- (45) Kaptan, H. Y. ESR Study on the Effect of Temperature on the Diffusion of Oxygen into PMMA and PVAc Polymers. *J. Appl. Polym. Sci.* **1999**, *71*, 1203–1207.
- (46) Shimada, S.; Kashima, K. Spin Label Study of the Factors Affecting Molecular Motion of Poly(Methyl Methacrylate). *Polym. J.* **1996**, *28*, 690–695.
- (47) Pace, M. D. EPR of C₆₀ Thermal/Photochemical Reactions with Polystyrene and Polymethyl Methacrylate. *Appl. Magn. Reson.* **1996**, *11*, 253–261.
- (48) Kobayashi, K.; Dochi, A.; Yajima, H.; Endo, R. ESR Studies of the Displacement Adsorption Behavior of Poly(Methyl Methacrylate) and Polystyrene System at the Solid–Liquid Interface. *Bull. Chem. Soc. Jpn.* **1993**, *66*, 1938–1943.
- (49) Ullman, E. F.; Call, L.; Osiecki, J. H. Stable Free Radicals. VIII. New Imino, Amidino, and Carbamoyl Nitroxides. *J. Org. Chem.* **1970**, *35*, 3623–3631.
- (50) Hirel, C.; Vostrikova, K. E.; Pécaut, J.; Ovcharenko, V. I.; Rey, P. Nitronyl and Imino Nitroxides: Improvement of Ullman's Procedure and Report on a New Efficient Synthetic Route. *Chem. – Eur. J.* **2001**, *7*, 2007–2014.
- (51) Wästlund, C.; Maurer, F. H. J. Positron Lifetime Distributions and Free Volume Parameters of PEO/PMMA Blends Determined with the Maximum Entropy Method. *Macromolecules* **1997**, *30*, 5870–5876.
- (52) Stoll, S.; Schweiger, A. EasySpin, a Comprehensive Software Package for Spectral Simulation and Analysis in EPR. *J. Magn. Reson.* **2006**, *178*, 42–55.
- (53) EasySpin, <http://www.easyspin.org/> (accessed April 20, 2021).
- (54) Birrell, G. B.; Van, S. P.; Griffith, O. H. Electron Spin Resonance of Spin Labels in Organic Inclusion Crystals. Models for Anisotropic Motion in Biological Membranes. *J. Am. Chem. Soc.* **1973**, *95*, 2451–2458.
- (55) Kobayashi, H. Inter-Spin Interactions of Organic Radical Chains in Organic 1D Nanochannels: An ESR Study of the Molecular Orientations and Dynamics of Guest Radicals. *Theoretical Chemistry for Advanced Nanomaterials -Functional Analysis by Computation and Experiment*, (Onishi, T., Ed.); Springer: Singapore, 2020, 423–467.
- (56) Freed, J. H. Theory of Slow Tumbling ESR Spectra for Nitroxides. *Spin Labeling, Theory and Applications*, (Berliner, L. J., Ed.); Academic Press Inc.: New York, US, 1976.
- (57) Bruce, S. D.; Higinbotham, J.; Marshall, I.; Beswick, P. H. An Analytical Derivation of a Popular Approximation of the Voigt Function for Quantification of NMR Spectra. *J. Magn. Reson.* **2000**, *142*, 57–63.
- (58) Tarasov, V. F.; Shkrob, I. A.; Trifunac, A. D. Spin-Polarized Nitroxide Radicals in Organic Glasses. *J. Phys. Chem. A* **2002**, *106*, 4838–4845.
- (59) Kobayashi, H.; Ueda, T.; Miyakubo, K.; Eguchi, T.; Tani, A. ESR Study of Molecular Dynamics and Orientation of TEMPO Included in Organic 1-D Nanochannel. *Phys. Chem. Chem. Phys.* **2008**, *10*, 1263–1269.
- (60) Kobayashi, H.; Asaji, T.; Tani, A. ESR Study of the Molecular Orientation and Dynamics of Stable Organic Radicals Included in the 1-D Organic Nanochannels of 2,4,6-Tris-4-(chlorophenoxy)-1,3,5-Triazine. *Magn. Reson. Chem.* **2012**, *50*, 221–228.
- (61) Kobayashi, H.; Aoki, K.; Asaji, T. Dynamics of TEMPOL Radicals in TPP 1D Nanochannels and Different Molecular Orientation from Other TEMPO Derivatives. *Chem. Lett.* **2015**, *44*, 893–895.
- (62) Tabak, M.; Alonso, A.; Nascimento, O. R. Single Crystal ESR Studies of a Nitroxide Spin Label. I. Determination of the g and A Tensors. *J. Chem. Phys.* **1983**, *79*, 1176–1184.
- (63) Jetti, K. R.; Thallapally, P. K.; Xue, F.; Mak, T. C. W.; Nangia, A. Hexagonal Nanoporous Host Structures Based on 2,4,6-Tris-4-(halo-phenoxy)-1,3,5-triazines (Halo = Chloro, Bromo). *Tetrahedron* **2000**, *56*, 6707–6719.
- (64) Allcock, H. R.; Siegel, L. A. Phosphonitrilic Compounds. III.1 Molecular Inclusion Compounds of Tris(o-phenylenedioxy)-phosphonitrile Trimer. *J. Am. Chem. Soc.* **1964**, *86*, 5140–5144.
- (65) Yamaguchi, D.; Eimura, H.; Yoshio, M.; Kato, T. Redox-active Supramolecular Fibers of a Nitronyl Nitroxide-based Gelator. *Chem. Lett.* **2016**, *45*, 863–865.
- (66) He, S. M.; Lei, Y. H.; Wang, J. M.; Geng, L. N.; Wang, S. P.; Zhao, J.; Hou, Y. F. The protective effect of nitronyl nitroxide radical on peroxidation of A549 cell damaged by iron overload. *Mater. Sci. Eng. C.* **2020**, *108*, 110189.

NOTE ADDED AFTER ASAP PUBLICATION

This paper published ASAP on August 4, 2021 with an error in the text. The manuscript was corrected and the revised version was reposted on August 6, 2021.